EarthArXiv preprint published at Environmental Research Letters (2019-04-26)
DOI: https://iopscience.iop.org/article/10.1088/1748-9326/ab13bf/meta

Extreme weather events in early summer 2018 connected by a recurrent hemispheric wave-7 pattern

Kai Kornhuber[1,2,*], Scott Osprey[1,2], Dim Coumou[3,4], Stefan Petri[3], Vladimir Petoukhov[3], Stefan Rahmstorf[3], Lesley Gray[1,2]

[1]Atmospheric, Oceanic and Planetary Physics, University of Oxford, Oxford, United Kingdom
[2]National Centre for Atmospheric Science, United Kingdom
[3]Earth System Analysis, Potsdam Institute for Climate Impact Research, Member of the Leibniz Association, Potsdam, Germany
[4]Institute for Environmental Studies, Vrije Universiteit Amsterdam, Amsterdam, Netherlands

*E-mail: Kai Kornhuber (kai.kornhuber@physics.ox.ac.uk)

EarthArXiv preprint published at Environmental Research Letters (2019-04-26)
DOI: https://iopscience.iop.org/article/10.1088/1748-9326/ab13bf/meta

Abstract

The summer of 2018 witnessed a number of extreme weather events such as heatwaves in North America, Western Europe and the Caspian Sea region, and rainfall extremes in South-East Europe and Japan that occurred near-simultaneously. Here we show that some of these extremes were connected by an amplified hemisphere-wide wavenumber 7 circulation pattern. We show that this pattern constitutes an important teleconnection in Northern Hemisphere summer associated with prolonged and above-normal temperatures in North America, Western Europe and the Caspian Sea region. This pattern was also observed during the European heatwaves of 2003, 2006 and 2015 among others. We show that the occurrence of this wave 7 pattern has increased over recent decades.

Keywords: Extreme Weather, Heat Waves, Rossby Waves, Teleconnections

1 Introduction

Extreme weather events such as heatwaves and floods are harmful to society and can lead to increased mortality, crop losses, and damage to infrastructure and economy (*1–3*). The European heatwave of summer 2003 is considered one of the most severe natural disasters in recent European history, with the number of excess deaths reaching tens of thousands and sizable losses to agricultural production across Europe (*1*). The persistent Moscow heatwave in July – August 2010 led to 55000 casualties and 30% crop-yield losses in Russia, whilst the Indus-River flood in Pakistan destroyed infrastructure and affected millions of people (*4, 5*). More recently, the record breaking heatwave of summer 2015 caused widespread water shortages, agricultural damages and wildfires throughout Europe (*6*).

While frequency and intensity of heat waves and heavy rainfall events are expected to increase in a warming world due to thermodynamic arguments (*7, 8*), the exact location and duration of these events are more uncertain and largely controlled by the atmospheric circulation, especially at mid-latitudes. Large-scale weather systems typically move eastward, but when the Jetstream strongly meanders this transport can come to a halt (*9*). Meanders in the jet are referred to as Rossby- or planetary waves and previous studies have pointed out that slow moving amplified planetary waves favor the occurrence of extreme weather conditions at mid-latitudes (*10–12*). Such quasi-stationary planetary waves can form (fully or nearly) circum-global teleconnections leading to the co-occurrence of unusual weather across the mid-latitudes (*13–18*). Moreover, the extreme heatwaves of 2003, 2010 and 2015 have been linked to high amplitude planetary waves. These heatwaves coincided with weather extremes occurring in other regions of the Northern Hemisphere (*12*).

Early summer 2018 witnessed several record-breaking and persistent heat and rainfall extremes occurring near simultaneously in the Northern Hemisphere (NH) mid-latitudes (*19–21*). These extremes include all-time temperature records measured in North America (e.g. Los Angeles and Montreal), in Western Europe (e.g. Glasgow, Belfast), the Caucasus (Tblisi, Yerevan) and Siberia as well as heavy rainfall in the Balkans and over Japan during two weeks in late June and early July.

EarthArXiv preprint published at Environmental Research Letters (2019-04-26)
DOI: https://iopscience.iop.org/article/10.1088/1748-9326/ab13bf/meta

Here we analyse the role of the atmospheric circulation in setting favorable locations of extreme weather events in early Summer 2018 and show that they were part of a recurrent wave-7 pattern (*18*). This wave-7 pattern is shown to constitute a recurrent teleconnection in Northern Hemisphere summer associated with persistent and above-normal temperatures in North America, Western Europe and the Caspian Sea region. We provide evidence that this pattern was also active during past episodes of extreme weather events, including the extreme summer heatwaves of 2003, 2006 and 2015 among others (*12*, *22*, *23*). Furthermore, we show that the identified pattern has increased in frequency and persistence over recent decades.

2 Data and Methods

Daily wind and temperature data were taken from the archives of the National Oceanic and Atmospheric Administration (NOAA, NCEP-NCAR reanalysis (*24*)). In order to avoid spurious trends due to the introduction of satellite-measurements in the late seventies, we limited the analysis to years 1979 – 2018. Wind fields and surface temperature anomaly fields are of a 2.5°x2.5° lat./lon. resolution and precipitation fields are 0.5°x0.5° resolution.

Phase velocities shown in Fig. 2e were determined using a fourth-order accurate numerical approximation of the transient derivative of phase based on daily data following Coumou et al. 2014 (3). In a second step 15-day running mean values of these daily phase velocities are calculated. Spectral decomposition of meridional wind at 300 mb to determine phase and amplitude of Rossby-waves was done using a fast Fourier transformation applied on the mid-latitude band averaged over 37.5° N – 57.5° N (*9*). The surface temperature composite anomaly field (Fig. 4a) was compiled using weekly temperature anomaly fields based on grid-point-wise detrended daily surface temperature fields. Statistical significance was assessed by comparing high amplitude events (>1.5 σ, where σ refers to standard deviation above mean) with the mean of all remaining weeks using a two sided t-test and an adjusted p-value determined by false discovery rate testing (FDR)(*25*).

3 Results

At the end of June, early July 2018 temperatures were anomalously high in specific regions of the Northern Hemisphere, namely the West-Coast of the US, Eastern Canada, western Europe including Scandinavia, the Central Asian regions around and to the North of the Caspian Sea and Siberia (Fig. 1a and Fig. 2a). Over the same time the mid-latitudinal upper tropospheric circulation was characterized by a strongly meandering jet that encircled the northern hemisphere in a regular pattern (Fig. 1b). The circulation regime of summer 2018 was remarkable, not only in terms of the amplitude and regularity of the wave-pattern but also due to its persistence, lasting for about 2 weeks from late-June to early-July.

EarthArXiv preprint published at Environmental Research Letters (2019-04-26)
DOI: https://iopscience.iop.org/article/10.1088/1748-9326/ab13bf/meta

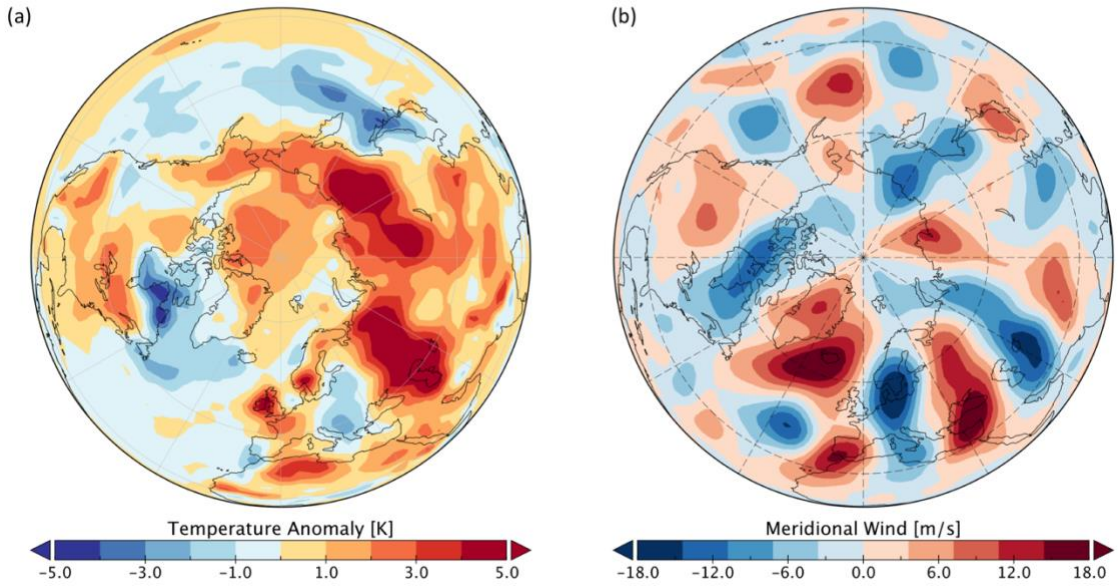

Figure 1. Northern Hemisphere temperature anomalies and stationary Rossby wave pattern in early July 2018. (a) Surface temperature anomalies (from 1981-2010 climatology; 15-day mean, centered on July 1st 2018). Oceans are masked in transparent grey. (**b)** As (a) but for meridional wind V (m s^{-1}) in the upper troposphere (250 mb). Dashed lines indicate the longitudes and latitudes grid at 30° separation.

Figure 2b shows the onset and persistence of the wave pattern as a Hovmöller plot (longitude vs. time) of the meridional winds averaged over the mid-latitudes (37.5°N-57.5°N, with the timing and longitude of persistent extreme weather events superimposed. Here, persistent heat extremes shown in Fig. 2b are defined using the 0.995 percentile threshold determined per grid-point based on detrended daily temperature anomalies (June-July 1979-2018, also see sensitivity analysis Fig.S11). Precipitation fields contain many 'zeros' and thus distributions of daily rain are highly skewed making thresholds based on percentiles challenging. Record statistics are commonly used when analysing precipitation extremes (*8*). Here we define precipitation extremes as the highest value measured at a grid-point in June-July 1979-2018. Only events that were persistent in time (i.e. meeting the extreme weather conditions for $t \geq 2$ days) in the mid-latitude (heat: 37.5°N – 57.5°N, rain: 35.25°N - 57.75°N) land-areas were considered.

In general, the westerly circulation is baroclinic, meaning that there is a displacement between the circulation at upper and lower pressure levels. However, during episodes of amplified planetary waves the atmospheric circulation can be considered as near-barotropic, thus circulation patterns are vertically aligned (*9*) (also see Fig. S12). In such a situation, the longitudinal position of southward and northward meridional winds in Fig. 2b can be understood as alternating troughs (southward followed by northward wind) and ridges (northward followed by southward wind) that relate to local cyclonic and anti-cyclonic circulation, respectively.

EarthArXiv preprint published at Environmental Research Letters (2019-04-26)
DOI: https://iopscience.iop.org/article/10.1088/1748-9326/ab13bf/meta

Consistent with this circulation, heat extremes (red diamonds in 2b) are generally located below a ridge, associated with anticyclonic conditions. In contrast, precipitation extremes (blue triangles) are generally below a trough, i.e. cyclonic conditions. While two thirds of the detected extremes are consistent with this description, there are some exceptions. Events not consistent with this behaviour include heat extremes over the North American west coast (~125°W) during June and over East Asia (~135°E in early June and the precipitation extremes over central North America mid-July (~120°W) and central Asia (~125°E) end of July. Relatively low meridional wind speeds in these regions suggest that these events might not be directly linked to the large-scale circulation (Fig. S6a). The mid-latitude circulation can be quantified in terms of Rossby waves by decomposing it into its principal wave components using a Fourier transformation (*10*, *26*). Starting at the end of June, a quasi-stationary wavenumber 7 (wave-7 from hereon) Rossby wave evolves (Fig. S3a, b) to large amplitude (Fig. 2b,c, Fig. S3c), near-stationary phase position (Fig. 2d) and near-zero phase speed (Fig. 2e). Although early Summer 2018 saw several persistent heat and rainfall extremes, simultaneous extremes in the mid latitudes occurred mostly during the period of amplified wave-7, specifically over the Eurasian continent (Fig. 2b). Those include the heat extremes over the British Isles, the rainfall extreme over SE Europe, the heat extreme over the Caspian Sea region and the heat extremes over Siberia (*19–21*). The precipitation extreme over Japan also occurring within this period was linked to an ex-tropical storm but was likely influenced by the large-scale circulation (see SI for details).

Wave-7 shows some unique behavior: it exhibits a persistent and preferred phase position when its amplitude increases (*18*) (also see Fig. S4), creating a circumglobal teleconnection pattern in NH summer (Fig. 3a,b). This is consistent with the work from Branstator et al. (*27*) and Ding and Wang (*16*) who showed that zonally elongated zonal winds (see Fig. S9) can act as waveguides for planetary waves leading to co-variability in far-away regions (*28*). The amplitude starts to increase from mid-June, exceeding the 1.5 standard deviation threshold by the end of June (Fig. 2c) and persists at that high level until early July. Concurrent with the rising amplitude, the wave shifts into its preferred phase-position (indicated by the dashed red lines in Fig. 2d, also see Fig. S4) where it persists for almost 3 weeks. The absolute phase speed of wave-7 thus slows down reaching almost zero when the wave enters its preferred phase position (Fig. 2e).

EarthArXiv preprint published at Environmental Research Letters (2019-04-26)
DOI: https://iopscience.iop.org/article/10.1088/1748-9326/ab13bf/meta

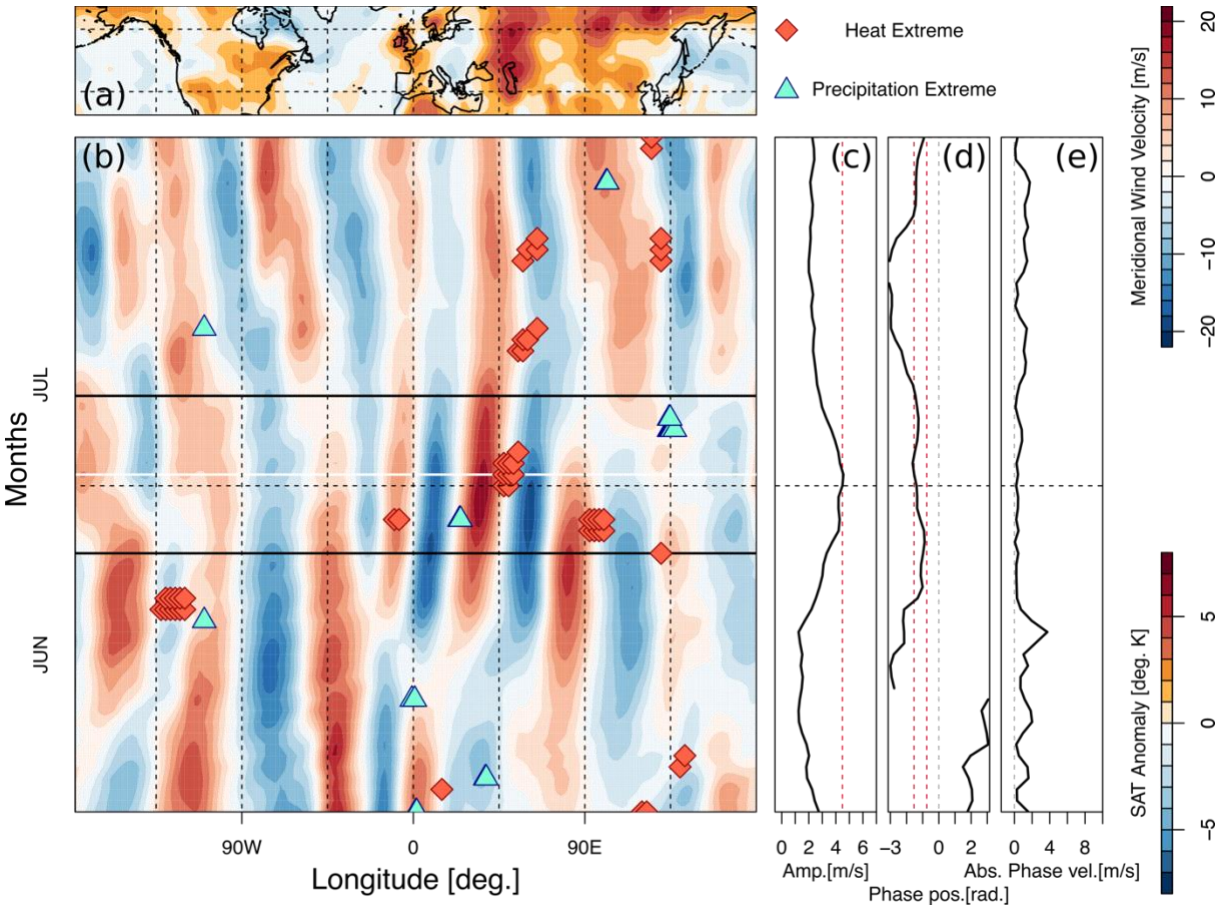

Figure 2. Time evolution of persistent wave-7 circulation pattern. (a) NH surface air temperatures (15-day mean centered on July 1st 2018). **(b)** Hovmöller (longitude-time) time evolution of the mid-latitude (averaged over 37.5°N – 57.5°N) 300 mb meridional winds. A stationary wave-7 pattern evolves during mid-June. The location and timing of persistent extreme events are marked by orange diamonds (heat extreme) and blue triangles (precipitation extreme). July 1st is marked by a horizontal white line, while the 15-day mean period is marked by horizontal black lines. The horizontal dashed lines mark the last day of June, while the vertical dashed lines separate the longitudes at 45° steps. **(c)** The amplitude of wave 7 increases and approaches the 1.5 σ (red dashed line) end of June / early July when heat records are broken across the mid-latitudes. **(d)** Phase of wave-7 (radians). The phase becomes locked within its preferred position (marked by red dashed lines) by end of June. **(e)** Phase speed of wave 7 (m s^{-1}). The phase speed slows down in concert with the increasing amplitude and the phase locking of wave-7.

The occurrence of this specific circulation pattern was not unique to June/July 2018. The hemispheric circulation associated with amplified wave-7 is a recurrent pattern observed in other years. As a consequence of its preferred phase, it exhibits spatially confined troughs and ridges which then persist over specific regions (Fig. 3) (*18*, *29*). A characteristic circumglobal pattern of alternating temperature anomalies thus arises across the mid-latitudinal belt with significantly elevated surface temperatures over central North America, Western/Central Europe and the Caspian Sea region (Fig. 3a). Here, high amplitude wave-7 events are defined by weeks in JJA where the amplitude exceeds the +1.5σ threshold (the pattern however is independent of the exact choice of threshold; see Fig. S5). In the regions identified above,

EarthArXiv preprint published at Environmental Research Letters (2019-04-26)
DOI: https://iopscience.iop.org/article/10.1088/1748-9326/ab13bf/meta

anomalous circulation arising from the wave-7 circumglobal teleconnection can then intensify the normal summer temperatures, contributing to heat waves on weekly to monthly time scales.

To quantify the similarity of the wave-7 pattern (Fig. 3b) with the mid-latitude meridional wind in 2018, we compute their hemispheric spatial correlation in the midlatitudes (57.5-37.5°N) also including separate sectors (Eastern hemisphere: 30W-150E, Western hemisphere: 150°E-30°W) (Fig. S2). During the phase-locked period (end of June, early July), the spatial correlations ρ peak above a level of 0.4, (statistically significant at the 99% confidence level) and remain over a threshold above 1.5 σ (Fig.S2c). Analysis of the separate sectors reveals that this is mainly due to the very high agreement over the eastern hemisphere (30W-150E, $\rho > 0.8$), although the western hemisphere nearly exceeds the 1.5σ threshold as well. In agreement with summer 2018, notable past amplitude wave-7 events coincide with heat extremes in central Western Europe and the Caspian Sea region as suggested by the surface temperature anomaly map (Fig. 3a), among them the heatwaves of 2003, 2006, 2012 and 2015 (*12*, *18*) (also see Fig. S6, Table S1).

Over recent decades the number of *phase-locked* wave-7 events (here defined as weeks with above average wave-7 amplitude within its preferred position, see Fig. S4) have increased significantly (95% confidence interval, Fig. 4b). Prior to 1999 there were no summers with two or more consecutive weeks of a wave 7 phase-locked circulation, but since then these have occurred (Table S2). Thus, the persistence of such situations appears to have increased. In fact, the average duration has doubled from about one to two weeks per year, while the number of years with more than two events per summer shows an almost eight-fold increase (Fig. S7). Although the trends are always upward, i.e. independent of the amplitude threshold used, their significance is sensitive to the amplitude threshold due to the reduction in ensemble size for high amplitudes (Fig. 4b). The number of wave-7 events (i.e. weeks with a high-amplitude wave-7 *irrespective* of its phase position) do not show statistically significant upward trends for different thresholds used (Fig. 4a). A statistically significant upward trend in the observed amplitude of summertime wave-7 is only detected when data from the pre-satellite period is included (Fig. S7). The more pronounced trends in *phase-locked* events (Fig. 4b), compared to high-amplitude events (Fig. 4a) suggests that it is the phase-locking itself that has increased. In general, these trends can simply reflect multi-decadal variability in the earth system given that the satellite record is relatively short. Nevertheless, an enhanced land-ocean temperature contrast as a consequence of amplified land warming provides a physical mechanism for such waves to become preferentially phase-locked. Such temperature contrast create an increased zonal temperature gradient at the coastlines and provide a stationary vorticity source that triggers and maintains atmospheric waves (*30*, *31*). It is therefore possible that the relative position of land and ocean areas in the mid-latitudes with high values of dT/dx over the continental West-coasts could favour a hemispheric wave 7 pattern (*32*). Such contrast would further enhanced by the cooling trend of northern Atlantic sea surface temperatures linked to a slowdown of the Atlantic Meridional Overturning Circulation (*33*) and implicated in past European heat extremes (*23*) but this needs further investigation.

EarthArXiv preprint published at Environmental Research Letters (2019-04-26)
DOI: https://iopscience.iop.org/article/10.1088/1748-9326/ab13bf/meta

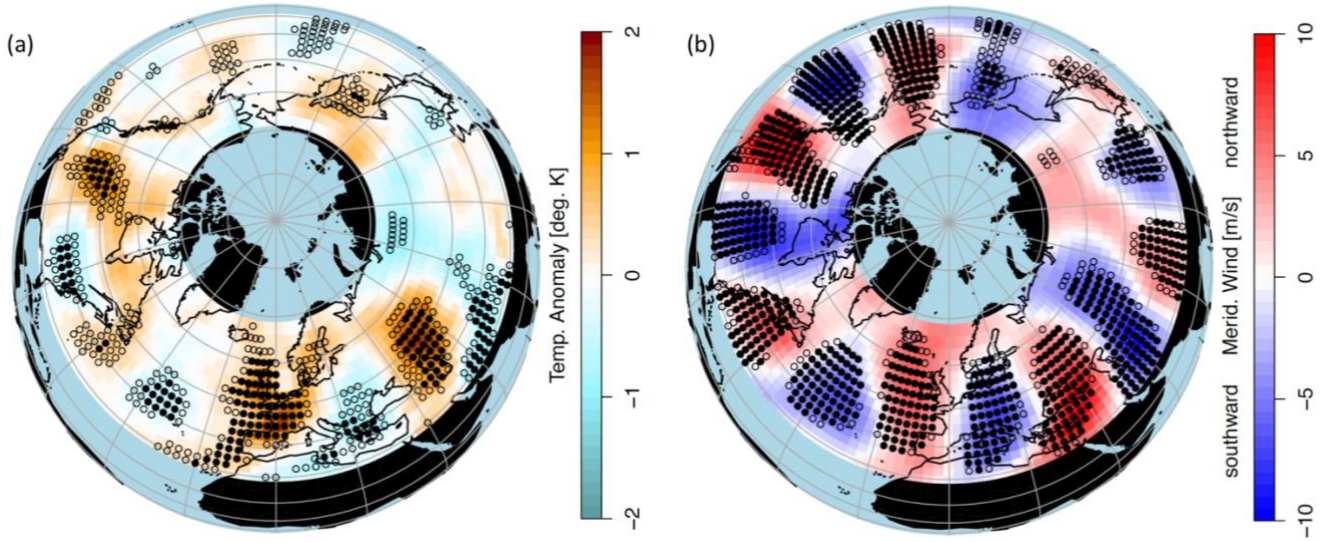

Figure 3. Composite plots of wave-7 events: A recurrent teleconnection. (a) Composite plot of surface temperature anomalies over the NH mid-latitudes (30°N - 67.5°N) during weeks of high wave-7 amplitudes (>1.5σ, N: 43 weeks, see Tab. S1) in summer (JJA) over the NH mid-latitudes (30°N - 67.5°N) observed over the period 1979 - 2017. **(b)** 300 mb meridional wind speeds (northward: red; southward: blue) during those events. The filled stippling in (**a**) and (**b**) indicates grid-cells with significant deviations from JJA climatology using a significance test that accounts for the false discovery rate (FDR) associated with multiple testing (*25*), while the grid-points marked with hollow stippling indicate local significance.

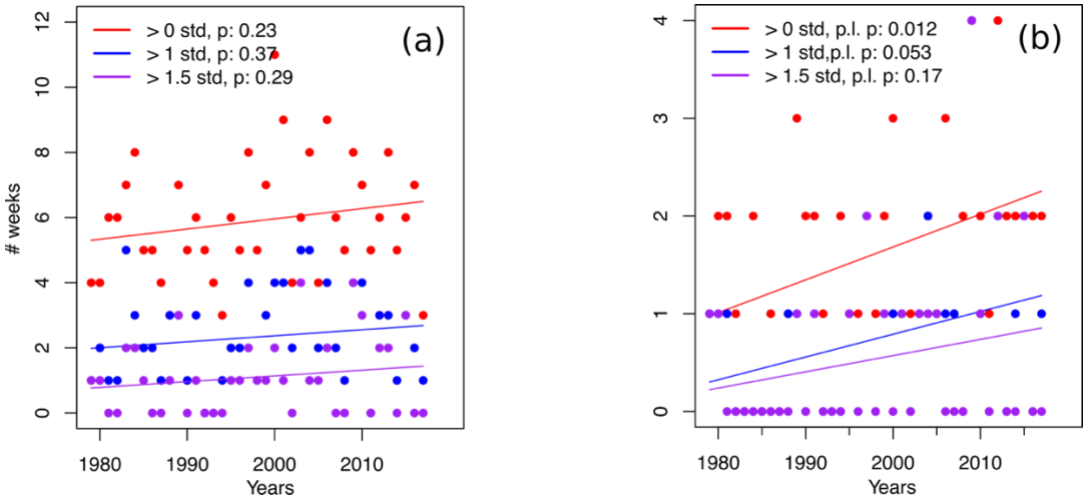

Figure 4. Recent trends in the occurrence of the wave-7 teleconnection. **(a)** Number of weeks per summer season (JJA, 1979-2017) with wave-7 amplitude above average (>0σ)**,** 1σ and 1.5σ irrespective of phase position. (**b)** Number of weeks per summer season (JJA) where wave-7 is in its preferred phase position (see Fig. S4) and the amplitude of wave-7 is above average (>0σ), >1 σ and >1.5σ.

EarthArXiv preprint published at Environmental Research Letters (2019-04-26)
DOI: https://iopscience.iop.org/article/10.1088/1748-9326/ab13bf/meta

4 Discussion

Extreme weather events such as the heatwaves observed in summer 2018 can be the product of several compounding factors acting together. For example it has been shown that the extreme heatwaves in Europe (2003) and Russia (2010) were preceded by very low soil moisture content due to an anomalously dry spring season (*22*, *34*, *35*). Similarly, during April-May 2018, soil moisture feedbacks may also have contributed to the magnitude and persistence of the observed heatwaves (*34*). Generally, heat waves are becoming more intense as the mean climate warms due to increasing greenhouse gas (GHG) concentrations (*36*). GHG warming also leads to enhanced water-holding capacity of the air (Clausius-Clapeyron), fueling heavier rainfall events(*8*). For these thermodynamic reasons, it is thus likely that the observed extremes in 2018 have in part been fueled by the global warming trend. However the timing, duration and location of a specific extreme weather event, can be largely controlled by the large scale circulation, especially at mid-latitudes (*37*).

While the direct response of weather extremes to thermodynamic drivers is generally well understood, large uncertainty remains of the indirect response from the changing atmospheric circulation under a warmer climate (*37–41*). Dynamical changes in the circulation have been proposed to explain the increase in persistence and magnitude of recent summer extremes that are otherwise unaccounted for using simple thermodynamic arguments (*41*, *42*). This arguments are particularly relevant in the case of Western and Central Europe as well as the Southern Central US being repeatedly struck by devastating heatwaves (*22*, *43–46*). Summer storm tracks have been weakening over recent decades (*47*) which likely influences planetary wave behaviour. In boreal summer the amplitude of synoptic Rossby waves (waves 5 and higher) have indeed been increasing recently, in agreement with our results (*48*). However, others studies have shown that upward trends over a relatively short period are difficult to assess (*49*) and traditional blocking indices also show no changes in summer (*50*).

The regions for which an increase in the persistence of regional weather regimes was identified (Europe and Western Asia) match those related to the wave-7 teleconnection pattern (*51*). Planetary wave resonance has been discussed as a potential mechanism to generate high amplitude synoptic wave patterns in boreal summer (*9*, *12*, *18*) and necessary conditions were present in June-July 2018 as well (also see discussion in SI). Recent trends in the zonal temperature profile due to anthropogenic climate change might favour resonance conditions (*32*). This temperature profile is characterized by enhanced land warming over high latitudes favouring the formation of an Arctic front jet, and subsequent double jet in the zonal mean (*12*, *32*). In fact, for 2018 such Arctic front jet is clearly visible over the Eurasian continent (Fig. S9), which might be the reason that planetary wave patterns were specifically amplified and persistent.

5 Conclusion

In summary, we have shown that the summer 2018 featured a series of nearly simultaneous extreme weather events that coincided in time and space with a circumglobal teleconnection constituted by an amplified Rossby wave (wave-7) in the mid-latitude jet stream specifically

over Eurasia. These extremes include the heat-records of June/July broken in Western Europe and Caspian Sea region, as well as the extreme and devastating rainfall events in South-East Europe. Tropical ENSO variability in 2018 was in a neutral state and thus unlikely to be an important factor behind the extreme weather events in the NH. This recurrent wave-7 circulation pattern conducive for heat waves acts in addition to the thermodynamically driven increase in heat, creating possibilities for very-extreme heat waves, specifically in the identified regions: Western Europe, North America and Caspian Sea region. We show that this circumglobal teleconnection pattern has increased in frequency and persistence in recent years. Given the high impacts of these extremes in terms of mortality, morbidity and agricultural losses, this presents major risks for society and global food production in particular, since the main breadbasket regions are located in the mid-latitudes. Further research is required to fully understand the combination of factors that trigger these observed wave events, and what determines their preferred phase position, so that predictability of future extreme events can be improved.

Acknowledgements

The federal state of Brandenburg is acknowledged for supporting the used high-performance computing resources. **Funding**: This work was supported by the UK Natural Environment Research Council (NERC) National Centre for Atmospheric Science (NCAS) and NERC grants NE/P006779/1 and NE/N018001/1 (K.K., L.G. and S.O.) and by the German Federal Ministry of Education and Research (BMBF) and by the Netherlands Organisation for Scientific Research (NWO) (D.C). **Author contributions**: K.K., S.O., D.C., L.G. conceptualised the paper. K.K. undertook the analysis. All authors contributed to the writing of the paper. **Competing Interests**: The authors declare no competing interests. **Data and materials availability**: The data used in this study can be obtained from NCEP-NCAR websites or via the UK Centre for Environmental Data Analysis (CEDA)

References:

1. D. Mitchell *et al.*, Attributing human mortality during extreme heat waves to anthropogenic climate change. *Environ. Res. Lett.* **11**, 74006 (2016).

2. C. Lesk, P. Rowhani, N. Ramankutty, Influence of extreme weather disasters on global crop production. *Nature*. **529**, 84–87 (2016).

3. L. Wenz, A. Levermann, Enhanced economic connectivity to foster heat-stress-related losses. *Sci. Adv.* **2**, e1501026 (2016).

4. D. Coumou, S. Rahmstorf, A decade of weather extremes. *Nat. Clim. Chang.* **2**, 1–6 (2012).

5. S. Russo *et al.*, Magnitude of extreme heat waves in present climate and their projection in a warming world. *J. Geophys. Res. Atmos.* **119**, 500–12 (2014).

6. NOAA, State of the Climate: Global Climate Report for 2015 (2016), (available at https://www.ncdc.noaa.gov/sotc/global/201513).

7. D. Coumou, A. Robinson, Historic and future increase in the global land area affected by monthly heat extremes. *Environ. Res. Lett.* **8**, 034018 (2013).

8. J. Lehmann, D. Coumou, K. Frieler, Increased record-breaking precipitation events under global warming. *Clim. Change*. **132**, 501–515 (2015).

9. V. Petoukhov, S. Rahmstorf, S. Petri, H. J. Schellnhuber, Quasiresonant amplification of planetary waves and recent Northern Hemisphere weather extremes. *Proc. Natl. Acad. Sci.* **110**, 5336–41 (2013).

10. J. A. Screen, I. Simmonds, Amplified mid-latitude planetary waves favour particular regional weather extremes. *Nat. Clim. Chang.* **4**, 704–709 (2014).

11. D. Coumou, V. Petoukhov, S. Rahmstorf, S. Petri, H. J. Schellnhuber, Quasi-resonant circulation regimes and hemispheric synchronization of extreme weather in boreal summer. *Proc. Natl. Acad. Sci.* **111**, 12331–12336 (2014).

12. K. Kornhuber, V. Petoukhov, S. Petri, S. Rahmstorf, D. Coumou, Evidence for wave resonance as a key mechanism for generating high-amplitude quasi-stationary waves in boreal summer. *Clim. Dyn.* **49**, 1961–1979 (2017).

13. K. Deng, S. Yang, M. Ting, A. Lin, Z. Wang, An Intensified Mode of Variability Modulating the Summer Heat Waves in Eastern Europe and Northern China, 361–369 (2018).

14. W. K. M. Lau, K.-M. Kim, The 2010 Pakistan Flood and Russian Heat Wave: Teleconnection of Hydrometeorological Extremes. *J. Hydrometeorol.* **13**, 392–403 (2012).

15. S. Saeed, N. Van Lipzig, W. A. Müller, F. Saeed, D. Zanchettin, Influence of the circumglobal wave-train on European summer precipitation. *Clim. Dyn.* **43**, 503–515 (2014).

16. Q. Ding, B. Wang, Circumglobal teleconnection in the Northern Hemisphere summer. *J. Clim.* **18**, 3483–3505 (2005).

17. H. Teng, G. Branstator, H. Wang, G. A. Meehl, W. M. Washington, Probability of US heat waves affected by a subseasonal planetary wave pattern. *Nat. Geosci.* **6**, 1056–1061 (2013).

18. K. Kornhuber *et al.*, Summertime Planetary Wave-Resonance in the Northern and Southern Hemisphere. *J. Clim.* **30**, 6133–6150 (2017).

19. NOAA, "State of the Climate: Global Climate Report for July 2018" (2018), (available at https://www.ncdc.noaa.gov/sotc/global/201807).

20. NOAA, "State of the Climate: Global Climate Report for June 2018" (2018), (available at https://www.ncdc.noaa.gov/sotc/global/201806).

21. International Federation of Red Cross and Red Crescent Societies, "Information Bulletin no. 1 Flash floods in Europe" (2018).

22. E. Black, M. Blackburn, G. Harrison, B. Hoskins, J. Methven, Factors contributing to the summer 2003 European heatwave. *Weather*. **59**, 217–223 (2004).

23. A. Duchez *et al.*, Drivers of exceptionally cold North Atlantic Ocean temperatures and their link to the 2015 European heat wave. *Environ. Res. Lett.* **11**, 074004 (2016).

24. Kalnay et al., The NCEP/NCAR 40-year reanalysis project. *Bull. Am. Meteorol. Soc.*, 437–470 (1996).

25. D. Wilks, " The Stippling Shows Statistically Significant Grid Points ." *Bull. Am. Meteorol. Soc.* **97**, 2263–2274 (2016).

26. D. Coumou, K. Kornhuber, J. Lehmann, V. Petoukhov, in *Climate Extremes: Patterns and*

Mechanisms, S.-Y. S. Wang, J.-H. Yoon, C. C. Funk, R. R. Gillies, Eds. (John Wiley & Sons, First Edit., 2017), pp. 61–73.

27. G. Branstator, Circumglobal Teleconnections, the Jet Stream Waveguide, and the North Atlantic Oscillation. *J. Clim.* **15**, 1893–1910 (2002).

28. G. Branstator, H. Teng, Tropospheric Waveguide Teleconnections and Their Seasonality. *J. Atmos. Sci.* **74**, 1513–1532 (2017).

29. J. Zhang, J. Yuanchun, C. Haishan, W. Zhiwei, Double-mode adjustment of Tibetan Plateau heating to the summer circumglobal teleconnection in the Northern Hemisphere. *Int. J. Climatol.* (2017), doi:10.1002/joc.5201.

30. T. A. Shaw, A. Voigt, Tug of war on summertime circulation between radiative forcing and sea surface warming. *Nat. Geosci.* **8**, 560–566 (2015).

31. B. J. Hoskins, D. J. Karoly, The Steady Linear Response of a Spherical Atmosphere to Thermal and Orographic Forcing. *J. Atmos. Sci.* **38**, 1179–1196 (1981).

32. M. E. Mann *et al.*, Influence of Anthropogenic Climate Change on Planetary Wave Resonance and Extreme Weather Events. *Sci. Rep.* **7**, 45242 (2017).

33. L. Caesar, S. Rahmstorf, A. Robinson, G. Feulner, Observed fingerprint of a weakening Atlantic Ocean overturning circulation. *Nature*. **556**, 191–196 (2018).

34. E. M. Fischer, S. I. Seneviratne, D. Lüthi, C. Schär, Contribution of land-atmosphere coupling to recent European summer heat waves. *Geophys. Res. Lett.* **34**, L06707 (2007).

35. D. G. Miralles, A. J. Teuling, C. C. van Heerwaarden, J. Vilà-Guerau de Arellano, Mega-heatwave temperatures due to combined soil desiccation and atmospheric heat accumulation. *Nat. Geosci.* **7**, 345–349 (2014).

36. D. Coumou, A. Robinson, Historic and future increase in the global land area affected by monthly heat extremes. *Environ. Res. Lett.* **8**, 034018 (2013).

37. T. G. Shepherd, Atmospheric circulation as a source of uncertainty in climate change projections. *Nat. Geosci.* **7**, 703–708 (2014).

38. J. Cohen *et al.*, Recent Arctic amplification and extreme mid-latitude weather. *Nat. Geosci.* **7**, 627–637 (2014).

39. E. A. Barnes, J. A. Screen, The impact of Arctic warming on the midlatitude jet-stream: Can it? Has it? Will it? *Wiley Interdiscip. Rev. Clim. Chang.* (2015) (available at http://doi.wiley.com/10.1002/wcc.337).

40. B. Hoskins, T. Woollings, Persistent Extratropical Regimes and Climate Extremes. *Curr. Clim. Chang. Reports*. **1**, 115–124 (2015).

41. R. M. Horton, J. S. Mankin, C. Lesk, E. Coffel, C. Raymond, A Review of Recent Advances in Research on Extreme Heat Events. *Curr. Clim. Chang. Reports*. **2**, 242–259 (2016).

42. J. Luterbacher *et al.*, European Seasonal and Annual Temperature Variability, Trends, and Extremes Since 1500. *Science (80-.).* **303**, 1499–1503 (2004).

43. A. Hoy, S. Hänsel, P. Skalak, Z. Ustrnul, O. Bochníček, The extreme European summer of 2015 in a long-term perspective. *Int. J. Climatol.*, 1–20 (2016).

44. M. Rebetez, O. Dupont, M. Giroud, An analysis of the July 2006 heatwave extent in Europe

compared to the record year of 2003. *Theor. Appl. Climatol.* **95**, 1–7 (2009).

45. M. Hoerling, J. K. Eischeid, X. Quan, T. Xu, Explaining the record US warmth of 2006. *Geophys. Res. Lett.* **34**, 1–4 (2007).

46. N. S. Diffenbaugh, M. Scherer, Likelihood of July 2012 U.S. temperatures in preindustrial and current forcing regimes. *Bull. Am. Meteorol. Soc.*, 6–9 (2013).

47. D. Coumou, J. Lehmann, J. Beckmann, The weakening summer circulation in the Northern Hemisphere mid-latitudes. *Science (80-.).* **348**, 324–327 (2015).

48. S.-Y. Wang, R. E. Davies, R. R. Gillies, Identification of extreme precipitation threat across midlatitude regions based on short-wave circulations. *J. Geophys. Res. Atmos.* **118**, 11059–11074 (2013).

49. J. A. Screen, I. Simmonds, Exploring links between Arctic amplification and mid-latitude weather. **40**, 959–964 (2013).

50. T. Woollings *et al.*, Blocking and its Response to Climate Change. *Curr. Clim. Chang. Reports*, 1–14 (2018).

51. D. E. Horton *et al.*, Contribution of changes in atmospheric circulation patterns to extreme temperature trends. *Nature*. **522**, 465–469 (2015).

EarthArXiv preprint published at Environmental Research Letters (2019-04-26)
DOI: https://iopscience.iop.org/article/10.1088/1748-9326/ab13bf/meta

Supporting Information for

Extreme weather events in early summer 2018 connected by a recurrent hemispheric wave-7 pattern

Kai Kornhuber [1,2,*], Scott Osprey [1,2], Dim Coumou [3,4], Stefan Petri [3],

Vladimir Petoukhov [3], Stefan Rahmstorf [3], Lesley Gray [1,2]

[1]Atmospheric, Oceanic and Planetary Physics, University of Oxford, Oxford, United Kingdom

[2]National Centre for Atmospheric Science, United Kingdom

[3]Earth System Analysis, Potsdam Institute for Climate Impact Research, Member of the Leibniz Association, Potsdam, Germany

[4]Institute for Environmental Studies, Vrije Universiteit Amsterdam, Amsterdam, Netherlands

*E-Mail: kai.kornhuber@physics.ox.ac.uk

EarthArXiv preprint published at Environmental Research Letters (2019-04-26)
DOI: https://iopscience.iop.org/article/10.1088/1748-9326/ab13bf/meta

Text S1. Japanese Floods early July 2018.

From late June through to early July the slow-moving circulation identified over Eurasia coincided with large high-pressure systems north and east of Japan (Fig. S1). This confined a north-east flow of warm moist air over Japan from lower latitudes. At the same time a seasonally stalled Meiyu weather front stretched across Japan causing persistent rainfall in the south-west Okinawa prefecture. These persistent rains were further exacerbated by the passage of ex-tropical storm Prapiroon over the affected areas, causing major flooding. A meandering atmospheric river of high moisture laden air is clearly evident in Fig. S1a at the time of this flooding event, which is clearly influenced by the background slow moving circulation patterns seen in Fig. S1b.

Text S2. Quasi-resonant amplification during June-July 2018.

Quasi-resonant amplification (QRA) was proposed as a dynamical mechanism that could lead to the high-amplitude planetary waves of synoptic scale wavenumbers 6-8 (*1*–*3*). The QRA mechanism as derived by Petoukhov et al. (*1*) assumes that 'a synoptic-scale free wave trapped in a midlatitude waveguide can resonate with the slow-moving forced wave and thereby increase its amplitude through a quasi-resonant amplification' (*3*). This framework thus differs from the concept of 'resonance' described in Held 1983 (*4*) as waves are not assumed to encircle the longitudinal belt to interact with the "tails" of themselves. The theory behind this mechanism is based on linear theory, and assumes a zonally symmetric background flow on which perturbations develop (*4*, *5*) but it only considers zonally elongated waves (in contrast to e.g. Hoskins & Karoly (*5*) who discuss meridionally propagating waves). It describes similar phenomena as Branstator et al. (*6*, *7*) who showed that circumglobal wave patterns can evolve when a waveguide is provided in zonal direction by a mid-latitudinal jet. A zonal waveguide effectively traps those waves in the mid-latitudes, preventing their dissipation in the meridional direction, which is the first precondition for QRA.

We tested the resonance conditions (Table S3) for the 2018 summer following the methodology of (2) (see Table S3 for details). Figure S9 provides evidence that the persistent wave 7 circulation pattern is consistent with the resonance of atmospheric waves trapped in a mid-latitude waveguide. It shows the time evolution of the prime quantities associated with wave resonance: The zonally averaged zonal wind U as a measure for the background flow (Fig. S9a), the squared meridional wavenumber (l^2) that determines waveguide formation (Fig. S9b) which is critical for resonance detection (Fig. S9c). A 'double jet' in the zonal mean jet evolves in early June (i.e. two peaks in U at ~45N and 75N). This configuration in the zonal mean zonal wind is characterized by a narrow subtropical jet with sharp edges which is known to favor waveguides (*8*). Figure S10 shows a 15-day average of the zonal wind field centered around the 1st July 2018. The zonal winds form a near circumglobal jet, which splits into a double jet configuration at 15W over Eurasia. A waveguide forms for wave 7 as indicated by the two turning points in l^2 (dotted black lines in Fig. S9b). The detection scheme also indicates sufficient orographic / thermal forcing and therefore resonance is detected from mid-June onwards (Fig. 2b, S9c). As expected from resonance theory, a few days later the phase speed of wave 7 slows down and the amplitude increases to a level above 1.5 {Merging Citations} deviations (Fig. 2d, e).

EarthArXiv preprint published at Environmental Research Letters (2019-04-26)
DOI: https://iopscience.iop.org/article/10.1088/1748-9326/ab13bf/meta

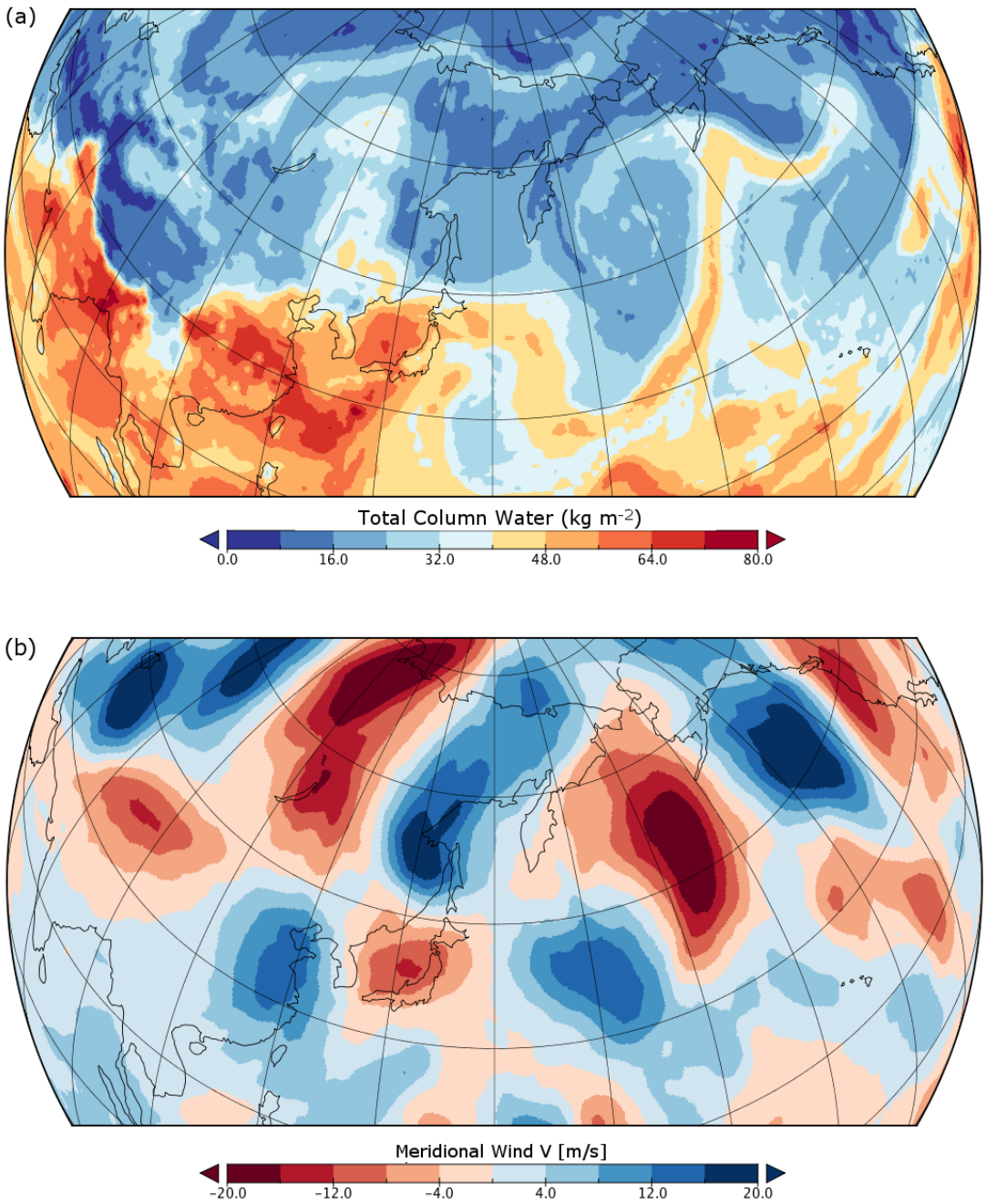

Figure S1. The role of the large-scale circulation in the Japanese Floods 2018. **(a)** Total column water measured 4th of July over the East Asian Pacific Sector **(b)** Meridional windspeeds centered on 4th July (7-day running average).

EarthArXiv preprint published at Environmental Research Letters (2019-04-26)
DOI: https://iopscience.iop.org/article/10.1088/1748-9326/ab13bf/meta

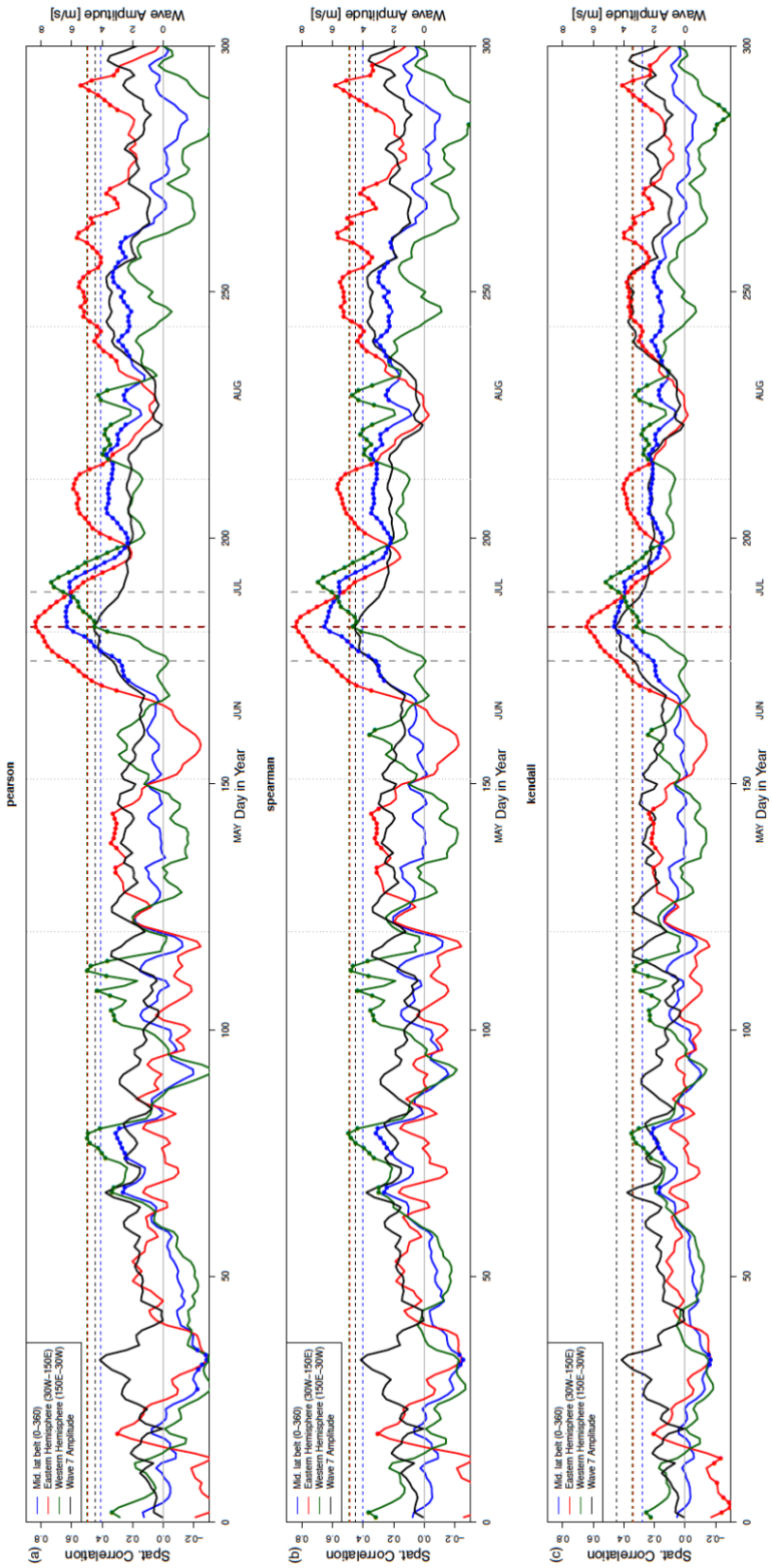

EarthArXiv preprint published at Environmental Research Letters (2019-04-26)
DOI: https://iopscience.iop.org/article/10.1088/1748-9326/ab13bf/meta

Fig. S2. Spatial correlation of v-wind field in 2018 and for wave-7 teleconnection pattern as a measure of similarity. **(a)** Pearson -, **(b)** Spearman -, **(c)** Kendall -Correlation coefficients based on the wave 7 teleconnection pattern (Fig. 3b) and mid. latitude (37.5-57.5) v-winds (blue solid line), Western hemisphere (150 E – 30 W, red solid line) and Eastern Hemisphere (30W-150E, red solid line). As orientation the wave 7 amplitude is provided (black solid line). The dashed horizontal lines indicate the 1.5σ above mean level respectively. The red vertical dashed line indicates the 1st of July while the grey vertical dashed lines give the 15-day period around that date. Dots on the lines indicate statistical significance (99% confidence level, null hypothesis: no correlation). Only every 3rd grid-point was included in order to account for autocorrelation. Months May – August are separated by grey vertical dotted lines. A 15-day running mean was applied on the wind fields.

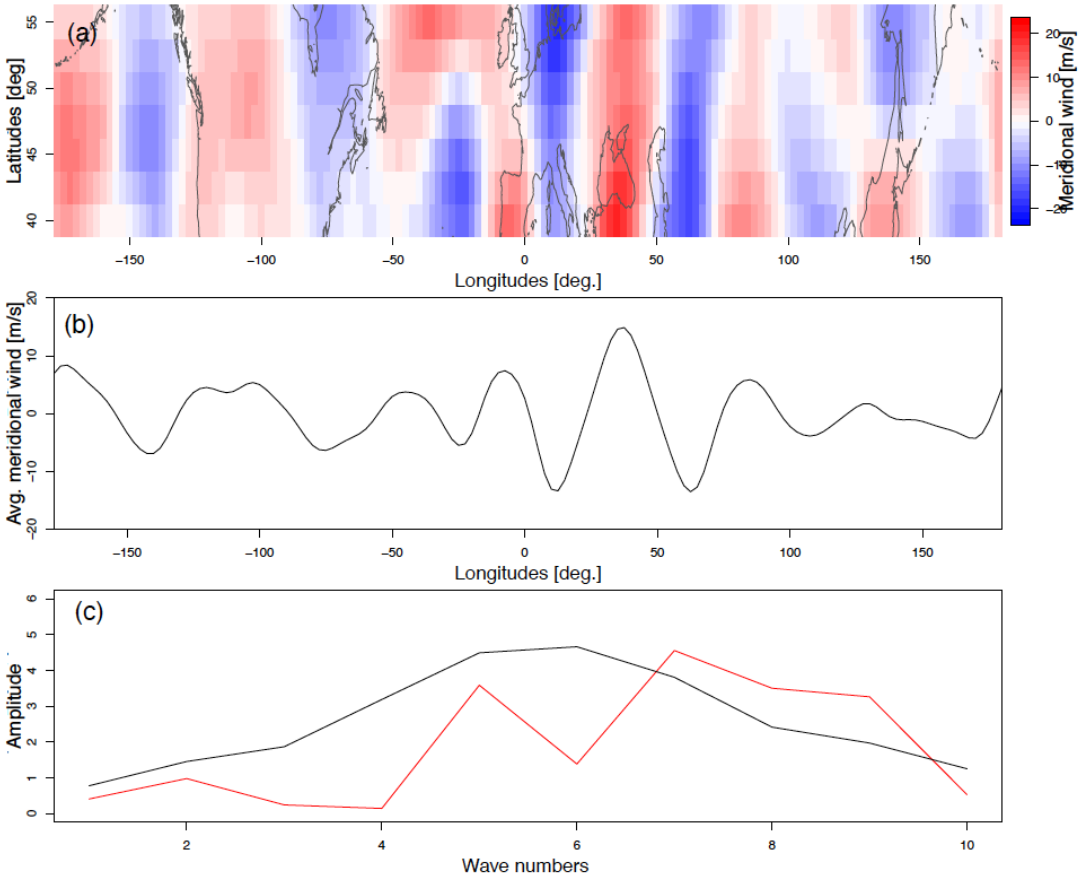

Figure S3. A circumglobal wave pattern during Jun-July 2018. (a) Meridional winds (15 day mean centered around the 1. Of July). **(b)** the meridional averaged meridional winds in the mid. latitudinal belt (37.5N-57.5N). **(c)** Rossby wave amplitudes of wavenumbers 1-10 determined by applying a Fast-Fourier-Transformation on the data shown in (b) (red curve) and their climatology (JJA, black curve). Wavenumbers above wave 6 are amplified, wave 7 dominates the spectrum.

EarthArXiv preprint published at Environmental Research Letters (2019-04-26)
DOI: https://iopscience.iop.org/article/10.1088/1748-9326/ab13bf/meta

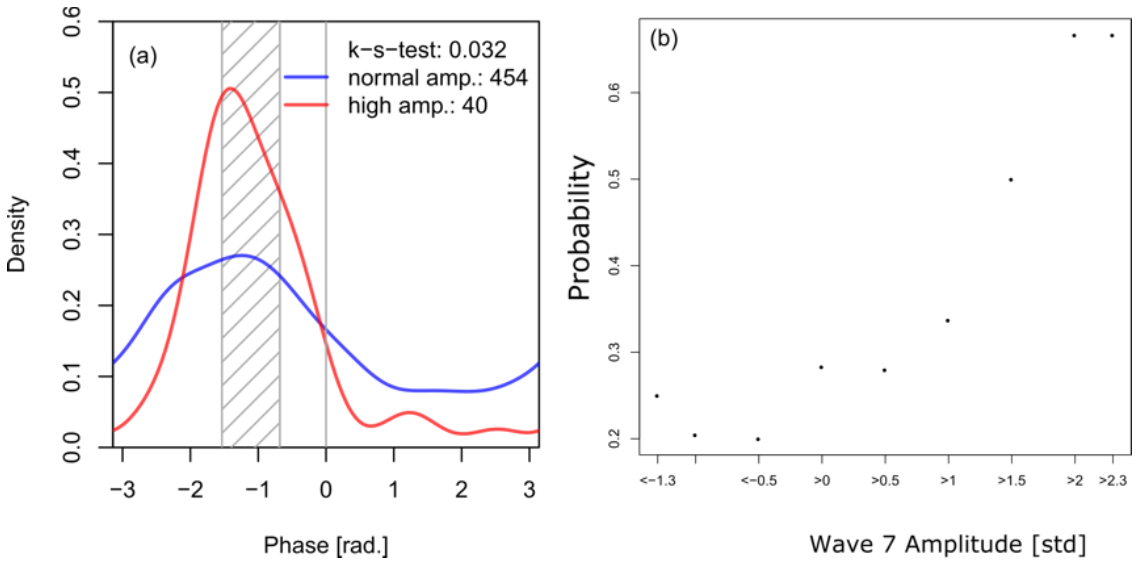

Figure S4. Phase locking of wave-7. (a) Probability density distributions during summer (JJA), comparing weeks of high amplitude (> 1.5σ, red) and normal amplitude (< 1.5σ, blue) of wave 7 **(b)** Probability of a week in summer (JJA) to exhibit phase of wavenumber 7 within the phase locked region as defined by the 25th -75th percentile of the high amplitude wave 7 (> 1.5σ). The probability increases with amplitude of wave 7.

EarthArXiv preprint published at Environmental Research Letters (2019-04-26)
DOI: https://iopscience.iop.org/article/10.1088/1748-9326/ab13bf/meta

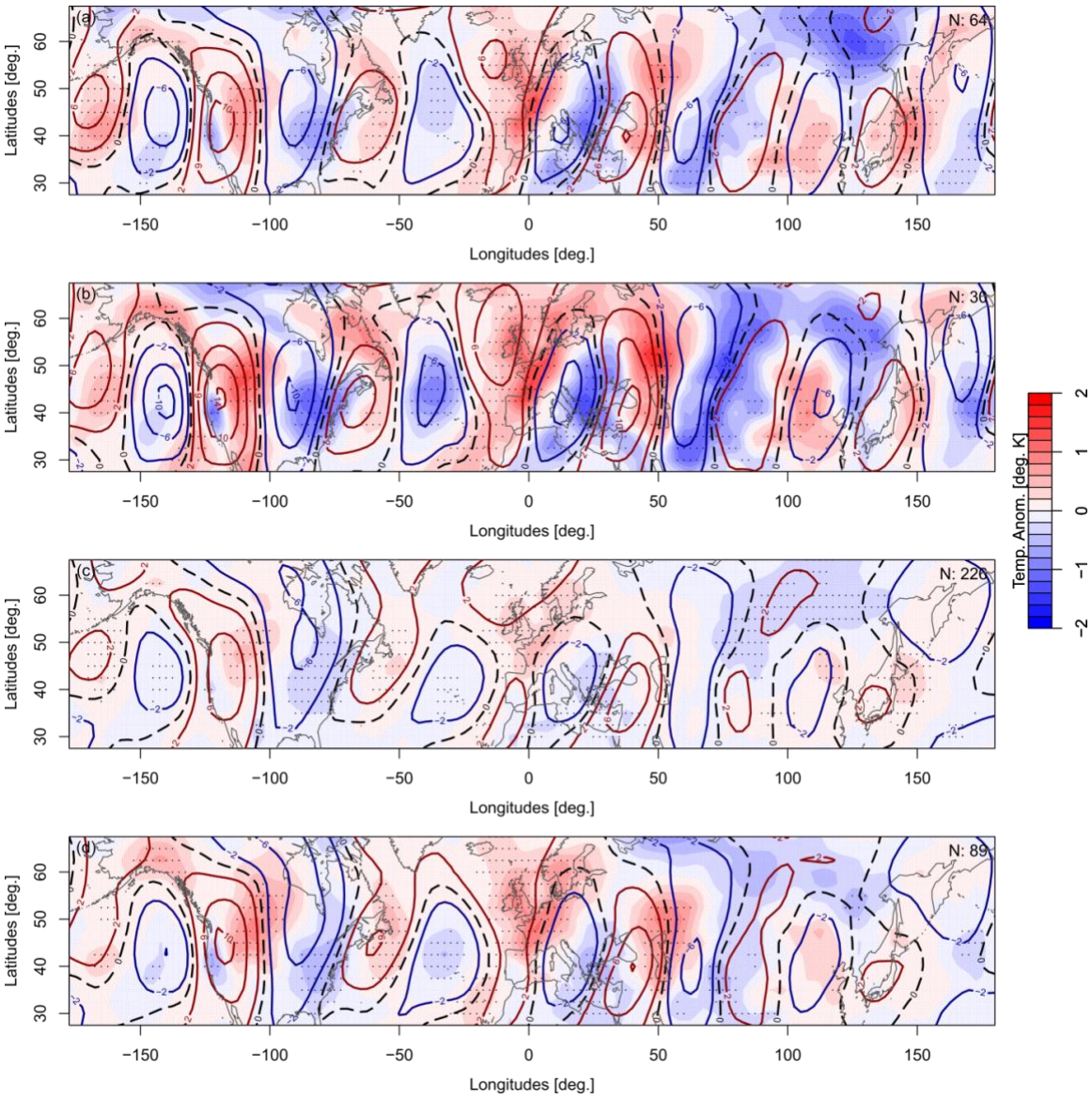

Figure S5. The recurrent wave-7 teleconnection. Composite temperature anomalies (filled contours) and meridional wind velocities (northward: red line contour, southward: blue line contour, zero wind line: black line) during weeks of wave-7 amplitude in summer (JJA, 1979 – 2016) **(a)** within the preferred phase position (see Fig.S3a, phase locked from here on) and above average, **(b)** phase locked and above 1σ, **(c)** above average irrespective of phase position, **(d)** above 1σ irrespective of phase position. Continental coastlines are depicted by grey outlines. The respective number N of averaged weeks is given in the upper right corner. Grey dots mark the grid-points where anomalies are significantly different (95% confidence level) from the remaining weeks. Note that unlike in Fig. 3a,b shown in the manuscript no false discovery rate significance testing (FDR(2)) was applied here.

EarthArXiv preprint published at Environmental Research Letters (2019-04-26)
DOI: https://iopscience.iop.org/article/10.1088/1748-9326/ab13bf/meta

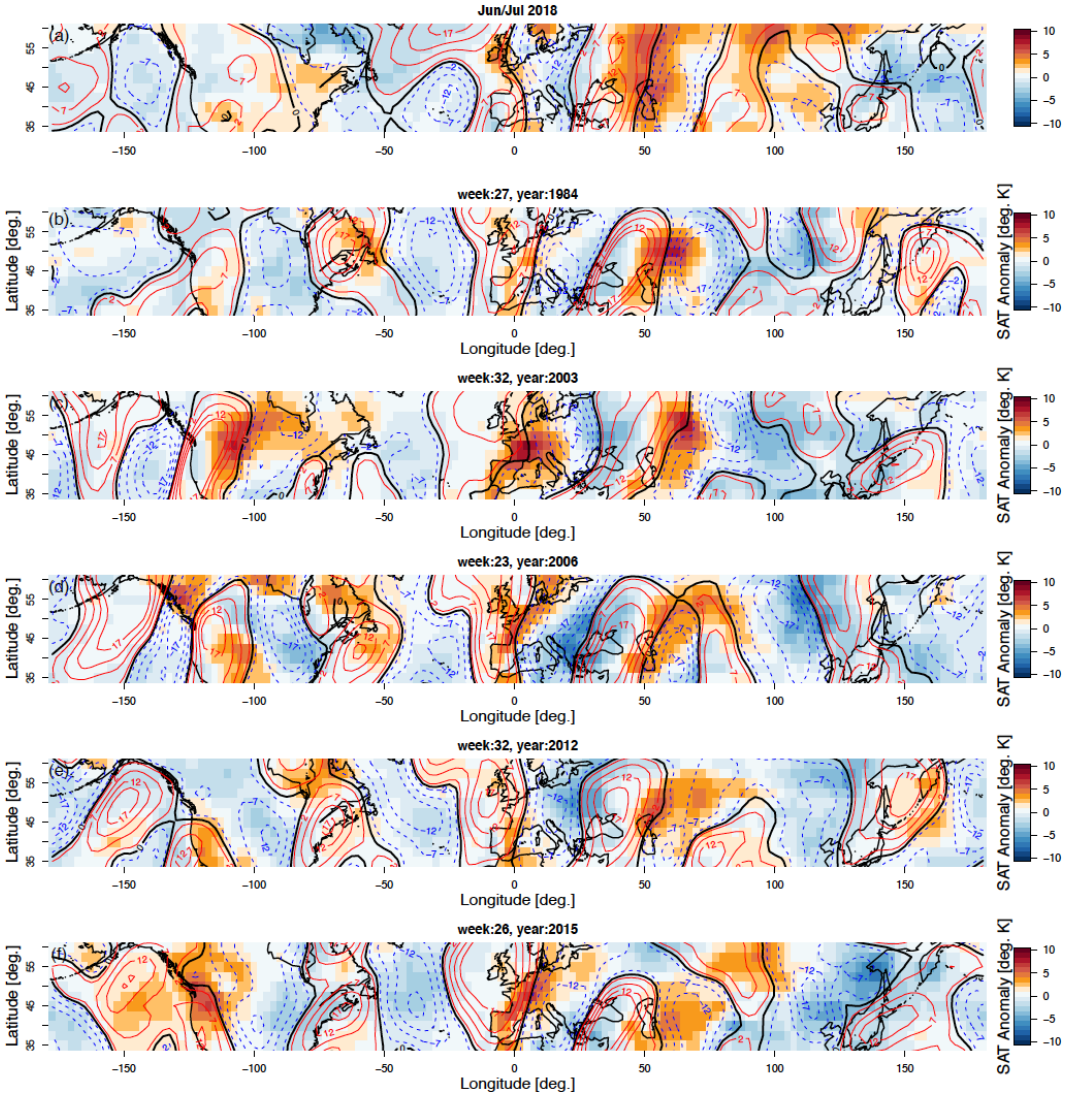

Figure S6. Hemispheric temperature and circulation extremes over the recent past. (a) Surface temperature anomalies (compared to 1981-2010 climatology, filled contours) and meridional winds (line contours, North-South: blue, South-North: red) in a 15-day running-mean centered around 1 July. **(b–f)** Same variables shown during selected examples of this pattern observed during summers of severe heatwaves in the Northern Hemisphere based on weekly means, including the severe European heatwaves of **(c)** 2003 and **(f)** 2015. For a full list see table S1.

EarthArXiv preprint published at Environmental Research Letters (2019-04-26)
DOI: https://iopscience.iop.org/article/10.1088/1748-9326/ab13bf/meta

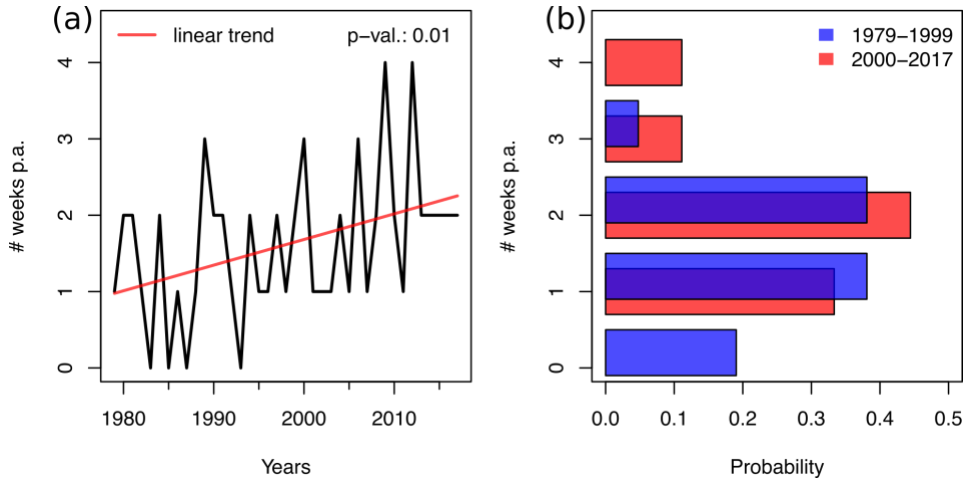

Figure S7. Trends in phase locked wave-7 events. (a) Number of weeks (JJA,1979 - 2017) with above average wave 7 amplitude in its preferred phase position (black line) with linear trend (red line: p-val. < 0.05) as shown in Fig. 4b. **(b)** Probabilities to see a certain number of weeks of an above average wave 7 in its preferred phase position, comparing years 1979 - 1999 (blue) and 2000 - 2016 (red).

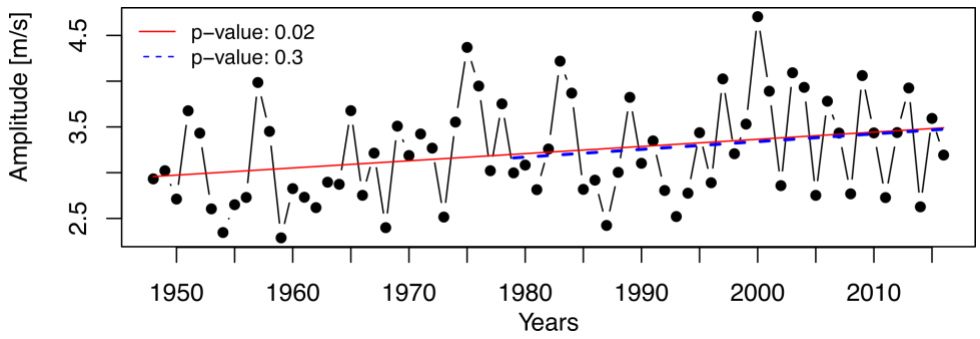

Figure S8. Long term trends in wave 7 amplitude. Mean wave 7 amplitude in summer (June-August) from over the period 1948 – 2016. Linear trends for the entire period (red solid line) statistically significant but might be spurious due to changes in measurement systems. Trends over the satellite-based measurement period (1979-2016) increasing but are not significant.

EarthArXiv preprint published at Environmental Research Letters (2019-04-26)
DOI: https://iopscience.iop.org/article/10.1088/1748-9326/ab13bf/meta

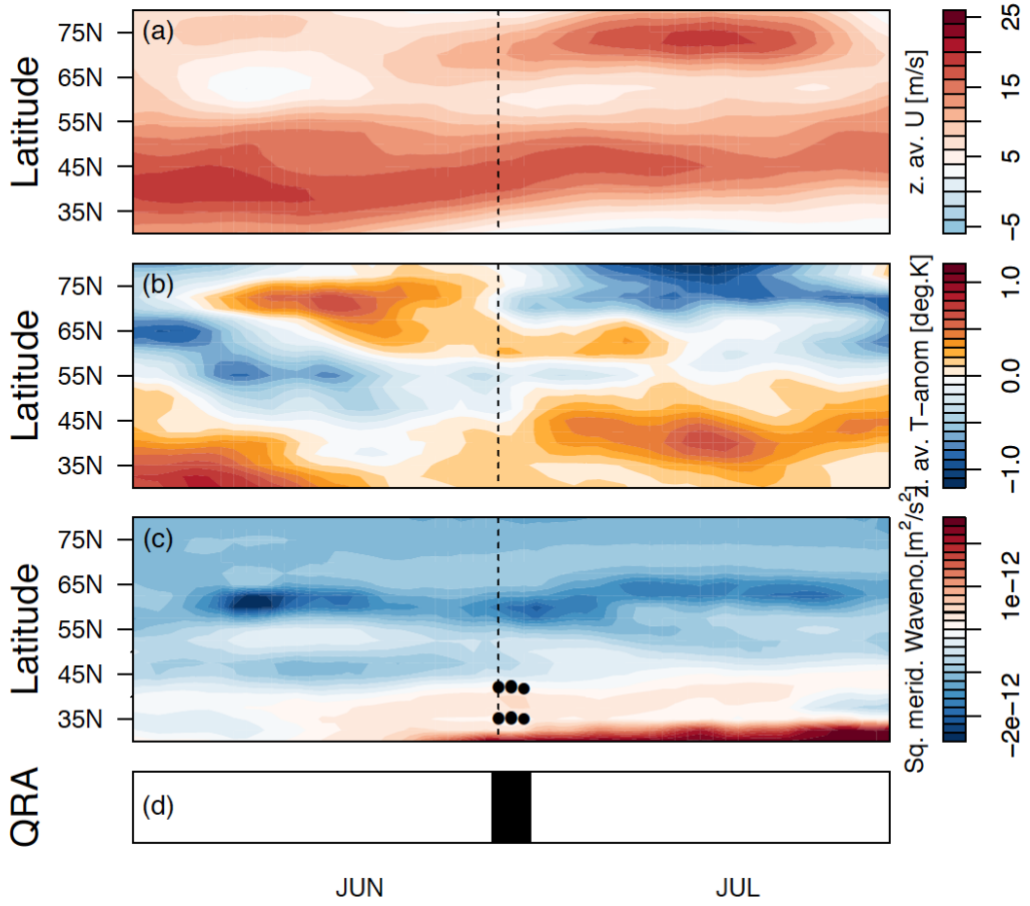

Figure S9. Resonance detection of wavenumber 7 early Summer 2018. (a) Time-series of zonally averaged zonal wind. A 'double jet pattern' forms at the beginning of June in the zonal mean. **(b)** Zonally averaged surface temperature anomalies (detrended). **(c)** Squared meridional wavenumber. A waveguide, the key condition for wave resonance, forms in end of June for wavenumber 7 and persists into early July, as shown by the black dots. **(d)** Resonance is detected from end of June on (marked in black).

EarthArXiv preprint published at Environmental Research Letters (2019-04-26)
DOI: https://iopscience.iop.org/article/10.1088/1748-9326/ab13bf/meta

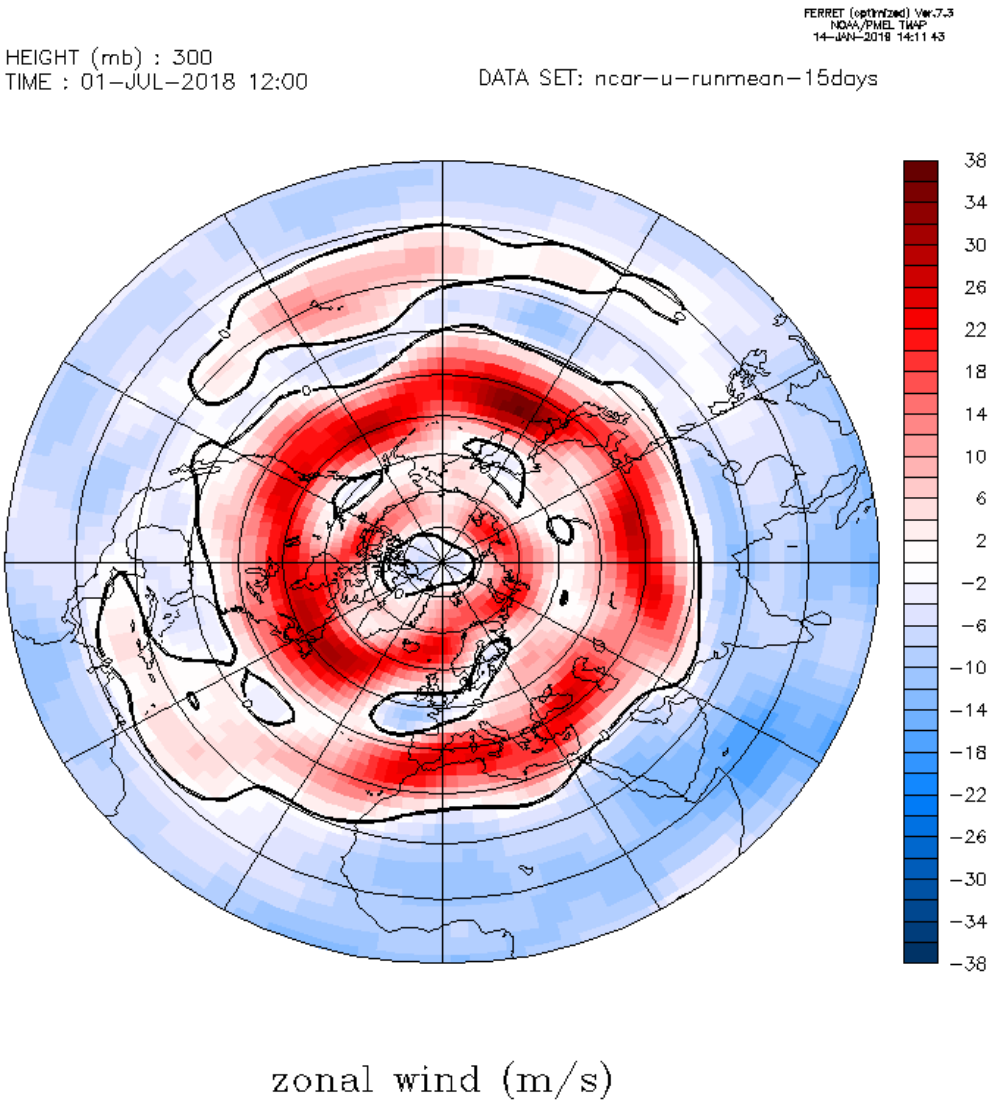

Figure S10. Zonal wind component in the upper troposphere. Shown is the 15-day mean, centered on July 1st 2018. A strong subtropical jet is visible over the entire longitudinal belt which splits into a double jet pattern over the Eurasian continent at about 15°W. The jet shows positive values around the entire hemisphere, thus providing a waveguide which can be considered circumglobal.

EarthArXiv preprint published at Environmental Research Letters (2019-04-26)
DOI: https://iopscience.iop.org/article/10.1088/1748-9326/ab13bf/meta

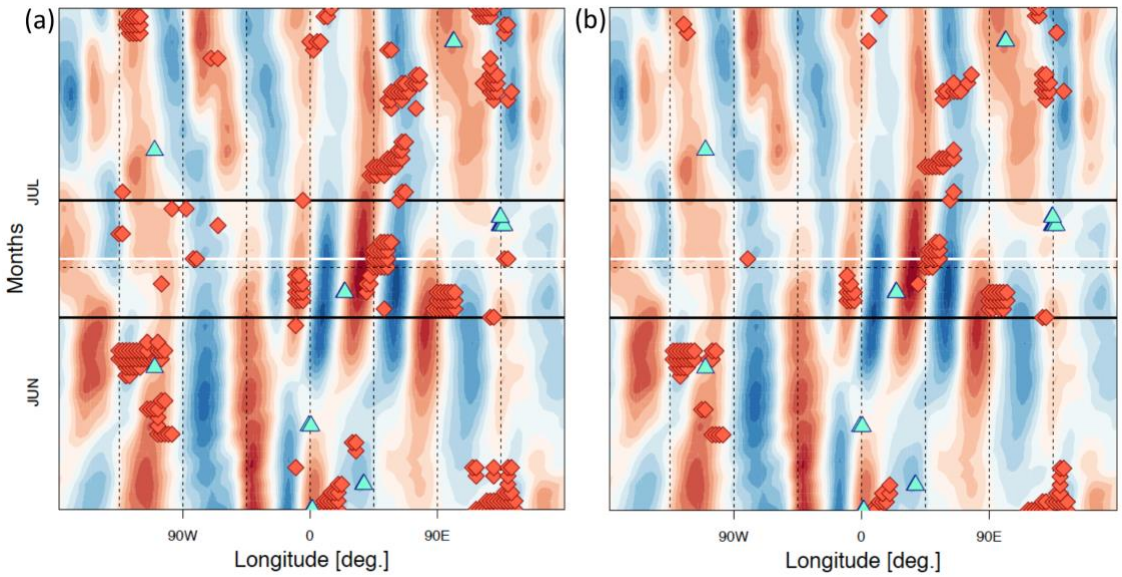

Fig. S11. Sensitivity Analysis of the employed heat extreme threshold. As Fig. 2b but for heat extremes defined by the **(a)** 0.975th and **(b)** 0.985th threshold. A lower threshold leads to more at extremes being detected. The patterns are mostly insensitive to the threshold, as most simultaneous heat extremes occur during the discussed period.

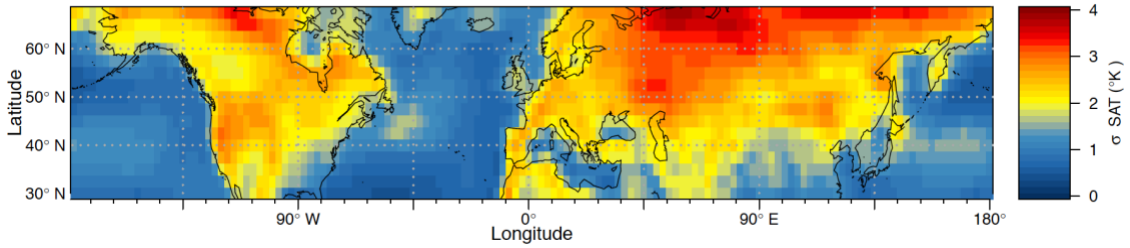

Fig.S12. June, July climatology of 1σ weekly mean near surface temperature anomalies.

EarthArXiv preprint published at Environmental Research Letters (2019-04-26)
DOI: https://iopscience.iop.org/article/10.1088/1748-9326/ab13bf/meta

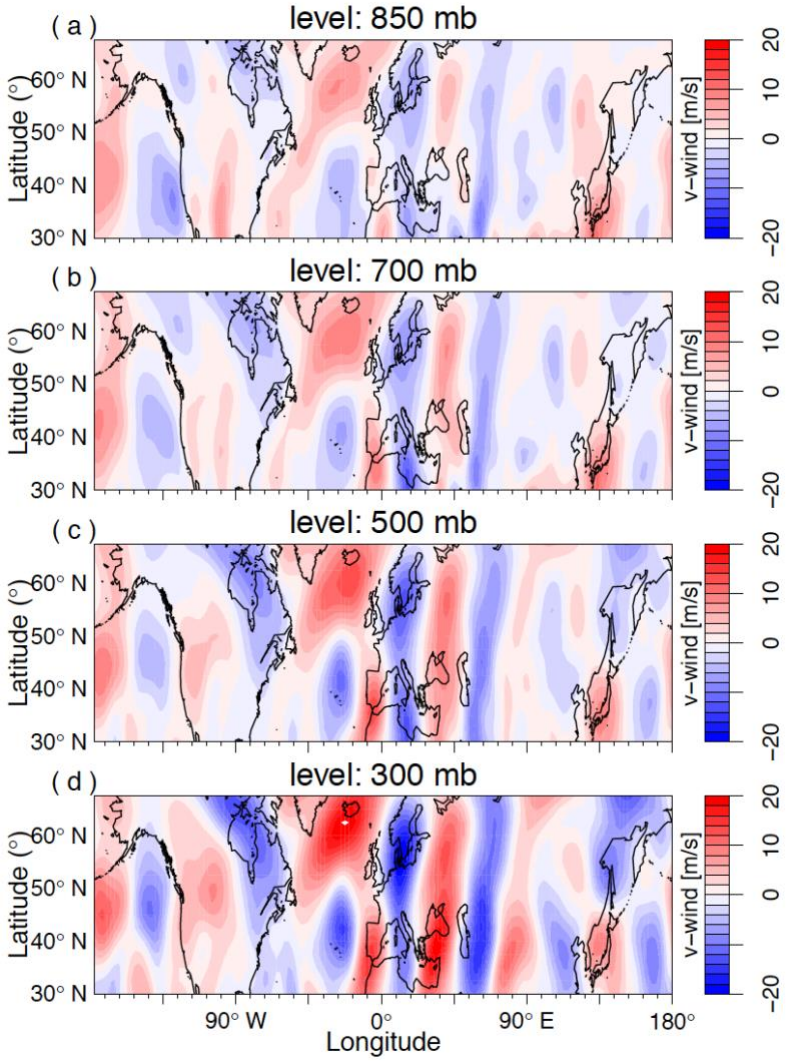

Fig. S13. Probing the barotropic structure. 15-day mean (centered around the 1st of July) northern hemisphere meridional wind fields in different pressure levels: **(a)** 850 mb, **(b)** 700 mb, **(c)** 500 mb and **(d)** 300 mb. The alignment of wind-patterns across pressure levels is an indication of a near barotropic circulation. Small deviations across pressure levels are observed over East Asia.

EarthArXiv preprint published at Environmental Research Letters (2019-04-26)
DOI: https://iopscience.iop.org/article/10.1088/1748-9326/ab13bf/meta

Table S1. Dates of 43 weeks with wave number 7 above 1.5σ, as used in the analysis shown in Fig. 3 a, b. Many occurrences coincide with heat extremes in regions outlined in Fig. 3.

No.	Date	No.	Date
1	29/06/1979	23	13/07/2003
2	31/05/1980	24	03/08/2003
3	06/07/1983	25	10/08/2003
4	13/07/1983	26	12/07/2004
5	14/06/1984	27	15/06/2005
6	05/07/1984	28	01/06/2006
7	29/06/1985	29	08/06/2006
8	28/06/1988	30	01/06/2009
9	15/06/1989	31	08/06/2009
10	13/07/1989	32	22/06/2009
11	27/07/1989	33	29/06/2009
12	17/08/1991	34	08/06/2010
13	06/07/1995	35	29/06/2010
14	12/07/1996	36	06/07/2010
15	01/06/1997	37	21/06/2012
16	24/08/1997	38	09/08/2012
17	03/08/1998	39	22/06/2013
18	27/07/1999	40	29/06/2013
19	28/06/2000	41	29/06/2015
20	19/07/2000	42	10/08/2015
21	22/06/2001	43	24/08/2015
22	06/07/2003		

EarthArXiv preprint published at Environmental Research Letters (2019-04-26)
DOI: https://iopscience.iop.org/article/10.1088/1748-9326/ab13bf/meta

Table S2. Dates of 63 weeks with wave number 7 amplitude above average, with the phase within its preferred phase position (see Fig. 4b, Fig. S7).

No.	Date	No.	Date	No.	Date
1	29/06/1979	22	14/06/1996	43	01/06/2009
2	31/05/1980	23	01/06/1997	44	08/06/2009
3	28/06/1980	24	24/08/1997	45	22/06/2009
4	27/07/1981	25	15/06/1998	46	29/06/2009
5	24/08/1981	26	20/07/1999	47	06/07/2010
6	24/08/1982	27	27/07/1999	48	27/07/2010
7	26/07/1984	28	31/05/2000	49	10/08/2011
8	16/08/1984	29	12/07/2000	50	21/06/2012
9	10/08/1986	30	09/08/2000	51	09/08/2012
10	31/05/1988	31	22/06/2001	52	16/08/2012
11	15/06/1989	32	20/07/2002	53	23/08/2012
12	20/07/1989	33	03/08/2003	54	06/07/2013
13	03/08/1989	34	12/07/2004	55	20/07/2013
14	08/06/1990	35	02/08/2004	56	13/07/2014
15	20/07/1990	36	15/06/2005	57	20/07/2014
16	22/06/1991	37	29/06/2006	58	29/06/2015
17	17/08/1991	38	06/07/2006	59	10/08/2015
18	07/06/1992	39	13/07/2006	60	07/06/2016
19	15/06/1994	40	13/07/2007	61	23/08/2016
20	03/08/1994	41	26/07/2008	62	08/06/2017
21	06/07/1995	42	23/08/2008	63	13/07/2017

EarthArXiv preprint published at Environmental Research Letters (2019-04-26)
DOI: https://iopscience.iop.org/article/10.1088/1748-9326/ab13bf/meta

Table S3. Key Conditions for resonance detection from (10)

i. *Waveguide for synoptic scale free wave k:*
1. Two turning points (TPs, change of sign) in l^2
2. $l^2 > 0$ between the turning points (TP)
3. $U > 0$ in between and in the vicinity of the TPs
4. The highest value of l^2 between the TPs is in the range of l^2_{min} and l^2_{max}
5. The TPs lie within a region of 30°N and 70°N
6. The TPs have a minimum distance of w_k
7. In case of two waveguides their distance has to exceed at least 5°
ii. *Effective Forcing Amplitude for forced planetary wave $m \approx k$:*
8. The effective forcing Amplitude A_{eff} for a respective wave number m has to exceed a certain threshold q_k, defined by the 50th percentile of the overall wave spectrum on a specific timestep.

EarthArXiv preprint published at Environmental Research Letters (2019-04-26)
DOI: https://iopscience.iop.org/article/10.1088/1748-9326/ab13bf/meta

References:

1. V. Petoukhov, S. Rahmstorf, S. Petri, H. J. Schellnhuber, Quasiresonant amplification of planetary waves and recent Northern Hemisphere weather extremes. *Proc. Natl. Acad. Sci.* **110**, 5336–41 (2013).

2. V. Petoukhov *et al.*, The role of quasi-resonant planetary wave dynamics in recent boreal spring-to-autumn extreme events. *Proc. Natl. Acad. Sci.* **113**, 6862–6867 (2016).

3. K. Kornhuber *et al.*, Summertime Planetary Wave-Resonance in the Northern and Southern Hemisphere. *J. Clim.* **30**, 6133–6150 (2017).

4. I. M. Held, in *Large-Scale Dynamical Processes in the Atmosphere*, B. J. Hoskins, R. P. Pearce, Eds. (Academic Press, 1983), pp. 127–168.

5. B. J. Hoskins, D. J. Karoly, The Steady Linear Response of a Spherical Atmosphere to Thermal and Orographic Forcing. *J. Atmos. Sci.* **38**, 1179–1196 (1981).

6. G. Branstator, Circumglobal Teleconnections, the Jet Stream Waveguide, and the North Atlantic Oscillation. *J. Clim.* **15**, 1893–1910 (2002).

7. G. Branstator, H. Teng, Tropospheric Waveguide Teleconnections and Their Seasonality. *J. Atmos. Sci.* **74**, 1513–1532 (2017).

8. I. Manola, F. Selten, H. De Vries, W. Hazeleger, "Waveguidability" of idealized jets. *J. Geophys. Res. Atmos.* **118**, 10432–10440 (2013).